Journal of Hazardous Materials 184 (2010) 574–584

Contents lists available at ScienceDirect

Journal of Hazardous Materials

journal homepage: www.elsevier.com/locate/jhazmat

Ageing and structural effects on the sorption characteristics of Cd^{2+} by clinoptilolite and Y-type zeolite studied using isotope exchange technique

I.A.M. Ahmed*, S.D. Young, N.M.J. Crout

School of Biosciences, Division of Agriculture & Environmental Sciences, University of Nottingham, Nottingham NG7 2RD, UK

ARTICLE INFO

Article history:
Received 22 February 2010
Received in revised form 13 August 2010
Accepted 19 August 2010
Available online 26 August 2010

Keywords:
Cadmium
First-order kinetics
Fixation
Diffusion
Isotopic exchange
Permeable Reactive Barriers

ABSTRACT

This research investigates the long-term kinetics of Cd^{2+} sorption and desorption by calcium-exchanged clinoptilolite (*CaCpt*) and Y-type (*CaY*) zeolite using isotopic exchange with ^{109}Cd while maintaining pH at circumneutral values. The effects of Si/Al ratio and crystal structure of these zeolitic materials on intracrystalline transport of Cd are discussed. A first-order kinetic model was developed to describe the progressive transfer of Cd^{2+} to a less reactive form within the zeolite structure, following initial sorption and subsequent desorption of Cd subject to different initial contact times. The kinetic model differentiates between two forms of sorbed Cd^{2+} designated 'labile' and 'non-labile' in which the labile form is in immediate equilibrium with the free Cd^{2+} ion activity in solution. A model combining diffusion and first-order kinetics for cation exchange was also employed to determine Cd^{2+} diffusivity and intracrystalline exchange rates in *CaY* and *CaCpt*. The efficiency of Permeable Reactive Barriers (PRBs) containing zeolitic materials in protecting water systems against lateral flow of metal-contaminated leachate was simulated for three contrasting zeolites. The slow transfer of Cd between labile and non-labile forms was particularly important in moderating high concentration pulses of Cd traversing the PRB. In addition, the reversibility of Cd fixation effectively restored the sorption capability of the zeolite through slow leakage to drainage water.

1. Introduction

The presence of toxic elements in aquatic environments is known to endanger public health and the natural ecosystem [1]. Over the past few decades, many organizations such as the U.S. Environmental Protection Agency (EPA) and World Health Organization (WHO) have developed regulatory guidelines for establishing acceptable exposure levels and concentration limits for many potentially hazardous elements [2,3]. These environmental regulations have provided an impetus for alternative remediation technologies while most businesses design engineered remediation systems based on cost and performance. Thus, technologies that utilize cost-effective and re-usable sorbents (e.g., zeolites) to remove toxic elements from wastewater and immobilize metals in soils are currently attracting a considerable attention.

Zeolites are crystalline inorganic polymers with a framework composed of an assembly of corner-shared TO_4 tetrahedral units, where T is either Si or Al, forming infinitely extending three-dimensional microporous networks. Their framework structure comprises cages and channels of molecular dimensions resulting in unique molecular sieving properties with pronounced selectivity of specific sorbed ions and molecules [4]. Negative charge in aluminosilicate zeolites arises from isomorphous substitution of Si^{4+} ions by Al^{3+} in the SiO_2 lattice. The resulting cation exchange capacity (CEC) is compensated by electrostatic adsorption of cations distributed among energetically different sites within the zeolite channel system [5]. It is known that as the Si/Al ratio (SAR) decreases, the thermal stability and acid resistance of zeolites also decrease [6]. These properties make zeolites attractive materials for many industrial and environmental applications including clean-up of trace metals and radionuclides from liquid effluents [7–10].

It is generally accepted that sorption of metal ions occurs in zeolites *via* a single reversible ion exchange mechanism [11–13] allowing zeolites to be reused several times with cycling between sorption and desorption processes. This partly explains the economic value of natural zeolites (e.g., clinoptilolite and chabazite) in industrial and environmental applications [14]. While the equilibrium properties of ion exchange reactions at mineral–electrolyte interfaces have been widely investigated, less information is available on the kinetics of these processes. The processes observed over short contact periods (minutes to days) are controlled by ion diffusion in the macropores of aggregated colloid particles or in concentrated suspensions [15]. However, only a few investigations of the slower exchange kinetics and desorption of trace metals with

* Corresponding author. Current address: The University of Lancaster, Lancaster Environment Centre, The Aquatic Chemistry Research Group, Bailrigg, Lancaster LA1 4YQ, UK. Tel.: +44 01524 510211; fax: +44 01524 593985.
E-mail address: i.ahmed@lancaster.ac.uk (I.A.M. Ahmed).

0304-3894/$ – see front matter © 2010 Elsevier B.V. All rights reserved.
doi:10.1016/j.jhazmat.2010.08.074

zeolites have been undertaken. A number of studies have reported 'irreversible' ion exchange of transition metal ions by X-, Y-, and A-type zeolites [16–18]. Other studies have shown that a small fraction of sorbed ions is 'partially irreversible' at room temperatures and the exchange of monovalent ions is faster than that of divalent ions [19,20]. Trgo and Perić [21] reported a gradual increase over 24 h in the release of K^+, Na^+, Mg^{2+}, and Ca^{2+} during ion exchange with Zn^{2+} on natural zeolites containing 50% clinoptilolite. Fletcher and Townsend [22] carried out short sorption and desorption experiments of metal ions on X-type zeolite and showed that variable amounts of Cd^{2+}, Cu^{2+}, Ni^{2+}, Co^{2+}, Mn^{2+} and Zn^{2+} were apparently bound irreversibly, whereas Ca^{2+} showed completely reversible ion exchange. Nery et al. [23] reported reversible exchange of Ca^{2+}, Cd^{2+} and Mn^{2+} and unusual irreversibility of Ba^{2+}, Sr^{2+} and Pb^{2+} in P-zeolite with ion exchange experiments carried out at 80 °C for 2–12 h. Significant irreversible exchange of Pb^{2+} in X-zeolite has also been reported [24].

It is noteworthy that most of the above sorption studies were carried out at short reaction times of a few hours to a few days and at high electrolyte concentrations (0.1–0.5 M). In some environmental applications, zeolites may be in contact with water for prolonged periods, as in Permeable Reactive Barriers (PRBs) where clean-up processes can take several months up to a few years, depending on factors such as groundwater flow rate. Therefore, kinetic studies that assess the risk of pollutant release, following initial sorption, and thereby indicate the long-term viability of remediation strategies with reactive materials, such as zeolites, are urgently needed. Furthermore, leachability of radionuclides from solidified products is one of the most important parameters in risk assessment and management of nuclear waste and thus quantitative long-term desorption experiments from zeolites are also required.

In a previous study [25] we demonstrated that Cd^{2+} showed time-dependent sorption by calcium-exchanged X-zeolite (*CaX*; SAR1.2) and wholly reversible exchange by Ca-exchanged chabazite (SAR3.0). In that study, prolonged isotopic exchange experiments (up to 100 d) were undertaken, which allowed discrimination between chemically reactive (labile) and non-reactive (non-labile) forms of Cd. In a more recent study [26], we employed Extended X-ray Absorption Fine Structure Spectroscopy (EXAFS) to show that the observed irreversibility in Cd sorption by *CaX* is caused by progressive migration of Cd^{2+} ions from sites in the large cavities into less accessible sites in the small cages of the *CaX* crystal. The purpose of this contribution is to present new data on the kinetics of Cd sorption and desorption in the slow-time domain (several days to months) by two zeolitic materials that have intermediate–high Si/Al ratios, that is, Y-type zeolite and clinoptilolite. Kinetic models describing the time-dependent sorption process are presented and mechanisms of Cd sorption in relation to zeolite crystal structure are discussed. In addition, the trend in Cd concentration in solution passing through a zeolite-containing PRB was modelled to investigate the potential role of reversible fixation in moderating the impact of short-term (100 d) pulses of high metal concentrations.

2. Materials and methods

2.1. Materials

The zeolitic materials used in this study were natural clinoptilolite and synthetic Y-type zeolites. Synthetic zeolites were supplied as a pure single phase with Na^+ as the only extra-framework cation. Clinoptilolite was dominated by Na^+ and K^+ and associated with 1–3% Fe oxides. The dithionite–citrate-bicarbonate (DCB)-extraction method [27,28] was used to remove crystalline and poorly ordered Fe-phases, and traces of free carbonates and organic matter. The concentration of DCB-extractable Fe (Fe_d) was determined using Flame Atomic Absorption Spectroscopy (F-AAS; Varian® SpectrAA-220-FS). At the end of the extraction procedure, clinoptilolite samples were washed with a solution composed of Na-citrate and NaCl to remove any dissolved Fe from the zeolite surface. The pH value of the aqueous suspension of the Na-exchanged Y-zeolites (*NaY*) was 9–10 whereas that of the Na-exchanged clinoptilolite (*NaCpt*) was close to neutrality. In order to avoid Cd precipitation (as $Cd(OH)_x^{2-x}$) and significant Cd^{2+} hydrolysis (e.g., formation of $CdOH^+$) at the high pH of the Na-exchanged zeolites, all zeolite samples were converted to the calcium form by dialyzing against 0.5 M $Ca(NO_3)_2$. Another reason for this choice is that Ca-exchanged zeolites are more resistant to hydrolytic decomposition than the Na-form in moderately acidic media [29]. Samples were washed briefly with Milli-Q water, freeze-dried overnight (Chemlab®, SB-4 model apparatus), and kept in closed polyethylene containers. The chemical composition of major constituents and trace elements (including Cd) of the as-received and the Ca-exchanged zeolites was determined by X-Ray Fluorescence spectrometry (XRF) using fused borate beads. Phase composition of the 'as-received' and Ca-exchanged zeolites was investigated using X-ray diffraction (XRD) using a CuKα source (40 kV and 20 mA) at a scanning rate of 0.6° min^{-1} in the 2θ range 3–70°. The cation exchange capacities (CECs) of zeolites were determined by exchange with ammonium nitrate at room temperature [30]. Prior to sorption experiments, stock suspensions of Ca-exchanged Y-zeolite (*CaY*) and clinoptilolite (*CaCpt*) were equilibrated in 0.01 M $CaCl_2$ for 2 weeks, maintained at a constant temperature of 22 °C and equilibrated with NH_3-free air. The pH of the equilibrated zeolite suspensions was measured before, and at the end of, this treatment.

The morphologies of zeolitic samples (*CaY* and *CaCpt*) were examined using a Field-Emission Gun Environmental Scanning Electron Microscope (FEG-ESEM) Philips XL30 with a specially designed cooling stage (*Peltier stage*) for controlling humidity of the sample. The particle size distributions of the *CaY* and *CaCpt* materials were first determined by analysing the ESEM micrograph and second using a laser diffraction technique using a Beckman Coulter LS230 laser particle analyzer which uses the polarization intensity differential scattering (PIDS) method.

2.2. Methods

2.2.1. Cd isotopic-exchange experiments

The concentration of labile and non-labile pools of Cd was determined for a series of contact times using a 'double-(isotopic)-labelling' technique previously used to study the kinetics of Cd fixation by X-zeolite and calcite [25,26,31]. The procedure involves (i) an initial addition of ^{109}Cd-labelled Cd to a mineral suspension, to follow progressive metal sorption, and (ii) periodic addition of a second (carrier-free) ^{109}Cd spike, to subsamples of the suspension, to determine changes in isotopically exchangeable Cd.

Cadmium (as $Cd(NO_3)_2$) was added to pre-equilibrated calcium-exchanged zeolite suspensions in 0.01 M $CaCl_2$ as a ^{109}Cd-spiked solution (i.e., a solution of ^{112}Cd labelled with ^{109}Cd to provide a specific activity of ~5.4 kBq μmol^{-1}). The solid phase loadings of Cd used were 0.2–12 mmol Cd kg^{-1} and the solid:solution ratios were 0.012 and 0.03 kg L^{-1} for *CaY* and *CaCpt*, respectively. Samples were gently mixed and left to equilibrate for 5–100 d at 22 °C. After a prescribed time, supernatant solutions were first separated by centrifugation at 2200 × *g* for 30 min and then filtered (<0.2 μm polyethersulfone membrane filter) and subsamples were withdrawn for ^{109}Cd radio-assay using a gamma-spectrometer with 3 × 3 in. NaI detector (Packard, COBRA-II). Results from the radio-assay were used to calculate the dissolved Cd (Cd_{soln}) and sorbed Cd (Cd_{TS}) according to Eqs. (1) and (2), respectively. The concen-

tration of isotopically exchangeable Cd (Cd_{LS}; μmol Cd kg^{-1}) was determined (Eq. (3)) by introducing a second spike (0.2 mL) of carrier-free ^{109}Cd (~14 kBq mL^{-1} in 0.01 M $CaCl_2$) directly to equilibrated suspensions after the determination of Cd_{soln} by radio-assay of the first spike. The concentration of non-labile or 'fixed' Cd, (Cd_{NL}; μmol Cd kg^{-1}) can be determined by difference from Cd_{TS} (Eq. (2)). This method was described in detail in our previous paper [25]. The pH values of the zeolite suspensions were measured at each sampling time and used together with Cd_{soln} to calculate the free Cd^{2+} ion activity $\{Cd^{2+}\}$ and to calculate the saturation indices of possible solid phases using the PHREEQC speciation model with the WATEQ4F thermodynamic database [32].

$$Cd_{soln} = \frac{A_{soln(1)}}{A^*} \quad (1)$$

$$Cd_{TS} = \frac{Cd_{Tot} - ((A_{soln(1)} \times V_{soln})/A^*)}{W} \quad (2)$$

$$Cd_{LS} = \frac{A_{solid(2)} \times Cd_{soln(2)}}{A_{soln(2)}} \quad (3)$$

In Eqs. (1)–(3), Cd_{Tot} is the total amount of Cd added to the system (μmol), A^* is the specific activity of the Cd stock solution (Bq μmol^{-1} Cd), V_{soln} is the volume of solution (L), W is the mass of zeolite (kg), $A_{soln(1)}$ is the radioactivity in the separated supernatant (Bq L^{-1}), $A_{soln(2)}$ (Bq L^{-1}) and $A_{solid(2)}$ (Bq kg^{-1}) are the amounts of radioactivity from the second spike of ^{109}Cd in the solution and solid phases respectively; the subscripts '(1)' and '(2)' represent measurements following the first and second spike of ^{109}Cd, respectively. The second spike of ^{109}Cd (carrier-free) mixes only with the readily exchangeable Cd in the zeolite. The chemically insignificant amount of Cd added in this spike does not alter the suite of site types involved in the equilibrium; it can only reflect the equilibrium already established between Cd^{2+}, Ca^{2+} (and H^+).

Following adsorption for a prescribed time, desorption experiments were carried out following the procedure described in our previous work [25,26]. Cadmium desorption was initiated by replacing ~50% of the supernatant solution with Cd-free desorbing solution (an aerated suspension of *CaY* or *CaCpt* in 0.01 M $CaCl_2$) and allowing samples to re-equilibrate over a period of 48 h. Supernatant samples were then separated for radio-assay as described before. This desorption procedure was repeated five times.

2.2.2. Measuring the concentration of dissolved Al and Si in zeolite suspensions

Supernatant samples of zeolite suspensions were separated by centrifugation at 2200 × *g* for 30 min followed by filtration (<0.2 μm PES filter). The concentration of dissolved Al was determined chemically in separated supernatants by FAAS (N_2O-C_2H_2) with the addition of an ionization buffer (2000 mg K L^{-1}) and a releasing agent (1000 mg La L^{-1}). The concentration of reactive silicate released from zeolites was determined using a standard molybdate colorimetric method [33,34].

2.2.3. Theoretical development

2.2.3.1. Two-state kinetic model (KM model). To obtain kinetic information on Cd sorption/desorption dynamics, we developed a model that defines the reactivity of sorbed Cd in terms of two states: designated labile (Cd_{LS}) and non-labile (Cd_{NL}). In this model, Cd_{LS} is assumed to be in constant dynamic equilibrium with the free ion activity of Cd^{2+}, $\{Cd^{2+}\}$, in solution, whereas Cd_{NL} is assumed to exchange with Cd_{LS} by a kinetically controlled process. Instantaneous partitioning between Cd_{LS} and Cd^{2+} is assumed to be governed either by a simple Freundlich (Eq. (4)) or Langmuir (Eq. (5)) equation.

$$Cd_{LS} = k_F\{Cd^{2+}\}^n \quad (4)$$

$$Cd_{LS} = \frac{k_L\, q_{max}\{Cd^{2+}\}}{1 + k_L\{Cd^{2+}\}} \quad (5)$$

The value of $\{Cd^{2+}\}$ at any time can be calculated from a mass balance of the total labile Cd (Cd_{TL}, μmol Cd kg^{-1}) measured by isotopic exchange:

$$\{Cd^{2+}\} = \left[Cd_{TL} - \left(k_F\{Cd^{2+}\}^n\right)\right] \times \left(\frac{W}{V_{soln} \times \theta}\right) \text{ based on Frendlich model} \quad (6)$$

$$\{Cd^{2+}\} = \left[Cd_{TL} - \left(\frac{k_F\, q_{max}\{Cd^{2+}\}}{1 + k_L\{Cd^{2+}\}}\right)\right] \times \left(\frac{W}{V_{soln} \times \theta}\right) \text{ based on Langmuir model} \quad (7)$$

where $\theta = Cd_{soln}/\{Cd^{2+}\}$, the constants k_F and n are Freundlich isotherm parameters and the constants k_L and q_{max} are Langmuir constants which reflect the affinity between metal ion and adsorbent and the maximum metal sorption capacity.

The transfer of Cd between labile and non-labile states is described by reversible first-order kinetics given by

$$\frac{d(Cd_{TL})}{dt} = -\frac{d(Cd_{NL})}{dt} = -k_1 Cd_{LS} + k_{-1} Cd_{NL} \quad (8)$$

where k_1 and k_{-1} are the first-order rate constants (d^{-1}) of the forward (sorption) reaction and the reverse (desorption) reaction, respectively. Note that k_1 and k_{-1} are phenomenological rate constants that account for both the diffusive transport and exchange of Cd between the internal zeolitic space and the bulk solution.

As the reaction approaches equilibrium the half-life ($t_{1/2}$; d^{-1}) for the reverse reaction can be calculated by

$$t_{1/2} = \frac{\ln(2)}{k_1 + k_{-1}} \quad (9)$$

The differential equation (Eq. (8)) was solved by a fourth-order Runge–Kutta procedure. A bisection method was used to solve Eq. (6) or Eq. (7) for $\{Cd^{2+}\}$. Estimation of the adjustable parameters (k_F, n, (or k_L, q_{max}), k_1, and k_{-1}) was carried out using a Levenberg–Marquardt procedure, which minimizes the residual standard deviation. All these numerical methods are described by Press et al. [35].

2.2.3.2. Simulation of Cd removal using zeolite-containing PRB. We assumed a water-saturated zeolite barrier of thickness Δx (m), effective porosity ε (dimensionless), density ρ (kg m^{-3}) with an incident and outgoing water flux of F (m^3 m^{-2} d^{-1}); (Fig. 1); water within the barrier was assumed to be uniformly mixed. This simplification allows exploration of the barrier's behaviour in the context of the chemical dynamics of the substrate but would not be suitable for hydraulic studies. These assumptions are applied to extend Eq. (8) to include Cd input and output terms to give Eq. (10) which was solved using the numerical methods described above:

$$\frac{d(Cd_{TL})}{dt} = -\frac{d(Cd_{NL})}{dt} = \frac{F}{\Delta x \rho} Cd_{in} - k_1 Cd_{LS} + k_{-1} Cd_{NL} - \frac{F}{\Delta x \rho}\{Cd^{2+}\} \quad (10)$$

where Cd_{in} (mg L^{-1}) is the Cd concentration of the incoming water flux. The term $F/\Delta x\rho$ represents the fractional turnover of the instantly and uniformly mixed water in the barrier per unit time.

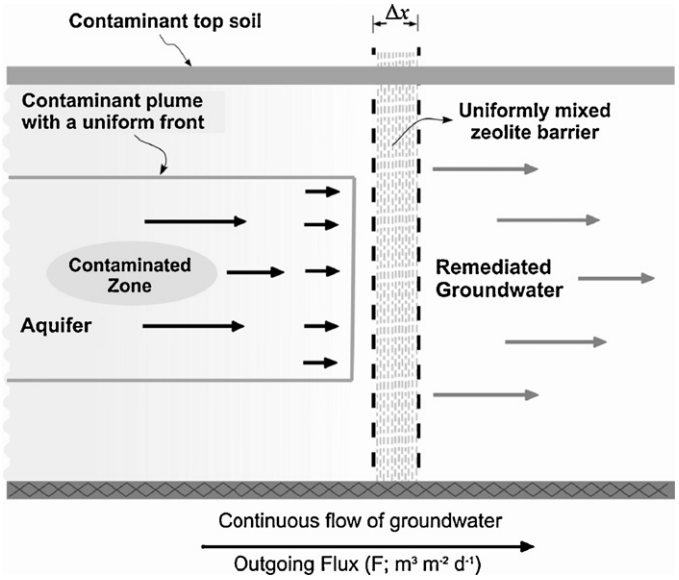

Fig. 1. A schematic drawing of the geometry of the PRB example with lateral flow of water at a flux (F) and thickness of the zeolitic barrier Δx.

2.2.3.3. Coupled ion exchange-diffusion model (CM model). Zeolites are cation exchangers that host both mobile and bound ions in their large channels. Equilibrium with ions in solution occurs when intra-zeolite bound ions exchange with mobile ions. Mobile ions migrate to or from solution by diffusion through the large cavities/channels. Both these two processes (i.e., sorption and diffusion) must be considered in any kinetic model of solid ↔ solution exchange. In our experiments, the zeolitic suspensions were kept under enhanced hydrodynamic conditions, by continuous mixing, which mean that the effect of liquid film diffusion was negligible and thus the focus in what follows is on the intracrystalline diffusion process. Brown and Sherry [39,40] and Baker et al. [36], studied isotopic exchange of Na^+ ions in hydrated NaX, NaA and NaY zeolites and showed that cation exchange is a two-step process in which the first step involves a fast migration of ions from large channels to the surface of zeolites. This step is diffusion-limited because diffusion through the large channels is slower than ion exchange. In the second step, mobile ions residing in large cavities exchange with bound ions inside small cages at a much slower rate. Note that both bound or unbound (mobile) cationic species can be present in large channels/cavities and these species will be in equilibrium with each other but are not necessarily at equilibrium with bound ions in small cages. Thus, ion transport to small ports in zeolites may occur through an intracrystalline exchange reaction mechanism rather than *via* a diffusion. This is in-line with our previous assumption (Eq. (8)) that the transfer of Cd between labile and non-labile states is a kinetically controlled process and leads to the following mechanism:

$$Cd_{soln} \xrightarrow{D_1} Cd_m \underset{\eta_2}{\overset{\eta_1}{\rightleftharpoons}} Cd_b \underset{\eta_4}{\overset{\eta_3}{\rightleftharpoons}} Cd_s \tag{11}$$

where Cd_m and Cd_b represent mobile and bound Cd^{2+} within large cavities while Cd_s represents bound Cd^{2+} in small cages, η_{1-4} are first-order rate constants for sorption and desorption processes, and D_1 is the diffusivity of mobile cations ($m^2\ s^{-1}$).

If ion exchange between Cd_m and Cd_b occurs instantaneously then Eq. (11) is reduced to

$$Cd_{soln} \xrightarrow{D} Cd_x \underset{\eta_6}{\overset{\eta_5}{\rightleftharpoons}} Cd_s \tag{12}$$

where Cd_x denotes both mobile and bound ions in large cavities, η_5 and η_6 are the corresponding sorption and desorption rate constants and D is the effective diffusivity of both mobile and bound ions where $D = D_1/(1+\alpha_{12})$ and α_{12} is an equilibrium constant = $Cd_m/Cd_b = \eta_2/\eta_1$. The analytical solution to resolve rate equations for the coupled diffusion and intracrystalline exchange is given by [37]:

$$U(t) = 1 - \frac{6}{\pi^2}\sum_{n=1}^{\infty}\frac{1}{n^2(u_n - v_n)}\left[u_n\left(1+\frac{v_n}{\zeta(1+\alpha)}\right)e^{v_n t} - v_n\left(1+\frac{u_n}{\zeta(1+\alpha)}\right)e^{u_n t}\right]$$

$$\text{where}\quad u_n = -\frac{1}{2}[(1+\alpha)\zeta + n^2 B_m]\left[1 - \left(1 - \frac{4\zeta n^2 B_m}{[(1+\alpha)\zeta + n^2 B_m]^2}\right)^{1/2}\right] \tag{13}$$

$$v_n = -\frac{1}{2}[(1+\alpha)\zeta + n^2 B_m]\left[1 + \left(1 - \frac{4\zeta n^2 B_m}{[(1+\alpha)\zeta + n^2 B_m]^2}\right)^{1/2}\right]$$

where $U(t)$ is the fractional attainment of equilibrium, B_m (diffusivity parameter) = $\pi^2 D_1/R^2(1+\alpha_{12})$, R is particle radius (m), n is an integer, ζ is a specific rate of exchange (in this case $\zeta = \eta_6$)and α is a constant = $\alpha_{23}\alpha_{12}/(1+\alpha_{12})$ where α_{23} is an equilibrium constant = $Cd_b/Cd_s = \eta_4/\eta_3$. If the exchange mechanism is purely diffusional then Eq. (13) reduces to Eq. (14) whereas if ions are trapped in the internal small cages or the site binding energy is very high then Eq. (13) reduces to Eq. (15):

$$U(t) = 1 - \frac{6}{\pi^2}\sum_{n=1}^{\infty}\frac{e^{-n^2 B_m t}}{n^2} \tag{14}$$

$$U(t) = \frac{1}{1+\alpha}\left\{1 - \frac{6}{\pi^2}\sum_{n=1}^{\infty}\frac{e^{-n^2 B_m t}}{n^2}\right\} \tag{15}$$

The model parameters (ζ, α, and D) in Eq. (13) were determined using the Nelder–Mead downhill simplex algorithm [35] written in Visual Basic programming language and called *via* an Excel macro.

Assuming that Ca^{2+} ions are initially the only bound ions in the internal space of a zeolitic phase Z then the symmetrical

Table 1
Origin, physical properties, and chemical composition of the as-received zeolitic materials used in this study.

Zeolitic material	Supplier	Origin	Surface area (N_2-BET) ($m^2\ g^{-1}$)	Particle diameter (μm)	Chemical composition (XRF)
Y-type	Zeochem AG, Switzerland	Synthetic	700	2–3 Sedigraph	66% SiO_2 22% Al_2O_3 13% Na_2O
Clinoptilolite	Euremica Environmental Ltd., UK	Natural, Australia	450	1000–2000 SEM	66% SiO_2 11% Al_2O_3 0.8% Na_2O; 3.4% K_2O 1.1% MgO; 2.9% CaO 1.6% Fe_2O_3 oxides

Table 2
The potential cation exchange capacity (CEC) and stoichiometric formulae of the unit cell of studied zeolites obtained from XRF.

Material	Stoichiometric formulae	CEC[a] ($mmol_c\ kg^{-1}$)	SAR[b]
Na-Clinoptilolite (NaCpt)[c]	$\lvert Ca_{0.4}Mg_{0.3}K_{1.4}Na_{3.2}\rvert[Al_6Si_{29}O_{72}]$	2630	4.8
Ca-Clinoptilolite (*CaCpt*)[c]	$\lvert Ca_{2.4}Mg_{0.1}K_{0.1}Na_{0.9}\rvert[Al_6Si_{29}O_{72}]$	2670	4.8
NaY	$\lvert Na_{54}\rvert[Al_{54}Si_{141}O_{384}]$	4220	2.6
CaY	$\lvert Ca_{20}Na_{14}\rvert[Al_{54}Si_{141}O_{384}]\rvert$	4258	2.6

[a] Estimation of theoretical CEC was based on anhydrous zeolite formulae.
[b] SAR, Si/Al ratio of zeolitic material.
[c] Composition following DCB-extraction: Fe_2O_3 was negligible (<0.04%) and thus excluded from clinoptilolite formulae.

Cd^{2+}–Ca^{2+} intracrystalline exchange can be written as $Cd^{2+}_{(aq)} + CaZ_{(ex)} \rightleftharpoons CdZ_{(ex)} + Ca^{2+}_{(aq)}$. The selectivity coefficient R_s for this reaction may take the form:

$$R_s = \frac{\gamma_{Cd}[CdZ]/\gamma_{Ca}[CaZ]}{\{Cd^{2+}\}/\{Ca^{2+}\}} \quad (17)$$

where braces denote aqueous activities and the square brackets denote molality of a cation in the zeolite phase; γ_{Ca} and γ_{Cd} are ion activity coefficients in the solid phase. Since Cd is present in the system in trace concentrations compared to Ca in the background electrolyte and Ca-exchanged zeolite then $\gamma_{Ca}[CaZ]/\{Ca^{2+}\} \approx$ constant and R_s is reduced to a modified distribution coefficient $K_d = \gamma_{Cd}[CdZ]/\{Cd^{2+}\}$. The term [CdZ] represents the sum of bound and mobile Cd^{2+} ions in the large cavities, which is equivalent to the value of $[Cd_{LS}]$ given in Eq. (4) or Eq. (5).

3. Results and discussion

3.1. Characterisation of studied zeolites

Initial investigation of the phase composition (XRF) of Y-zeolites indicated high phase purity (Table 1) and the absence of organic contamination whereas those of clinoptilolite were ~80% pure with 1.6% (by weight) as Fe oxides. The concentration of DCB-extracted Fe from *NaCpt* was ~1.3 mmol Fe kg^{-1}. The objective of the Fe extraction procedure was mainly to avoid specific Cd adsorption on Fe^{III} (hydr)oxides. The DCB-extraction also released ~0.5 mmol Al kg^{-1} and <1.0 μmol Si kg^{-1} from *NaCpt*. This amounted to <0.03% of the total Al or Si content and suggests that negligible structural damage of the zeolite had occurred. The chemical composition and the Si/Al ratio of treated Ca-exchanged clinoptilolite (*CaCpt*) given in Table 2 were similar to that before the DCB-treatment. The extraction of isomorphologically exchanged Fe^{3+} from the zeolitic framework is possible but our data suggest that the proportion of structural Fe^{3+} was negligible. XRD data (Fig. S1, supplementary data) of *CaY*, and treated clinoptilolite samples suggested that Ca-exchange resulted in no significant changes in the structure or the framework composition (i.e., Si/Al ratio) of the zeolite samples. Analysis of Al and Si released during the Ca-exchange process confirmed that the zeolite framework composition remained unchanged. Data in Table 2 shows that 74% and 60% Ca-exchange was achieved in *CaY* and *CaCpt*, respectively. Incomplete cation exchange of these zeolites is well documented elsewhere [16,17,38] and confirms the difficulty in removing tightly bound Na^+ or K^+ ions. The pH of air-equilibrated *CaY* and *CaCpt* suspensions before starting sorption experiments was 7.3 and 6.94, respectively. Variations in suspension's pH after the addition of Cd or during sorption/desorption experiments were small (<0.2).

The average particle radii (assuming spherical geometry) of *CaY* and *CaCpt* particles obtained from analysing ESEM images and laser diffraction method were 24 and 46 μm, respectively.

3.2. Kinetics of cadmium sorption and desorption on synthetic Y-type zeolite (CaY)

CaY zeolite showed rapid Cd sorption in the initial stages (<5 d) of the reaction with >75–80% of Cd removed from solution (Fig. 2). A progressive increase in Cd sorption by *CaY* up to 40 d was evident. As shown in Fig. 3, Cd desorption was characterised by marked hysteresis confirming non-reversible Cd sorption on *CaY*. The relationship between labile sorbed Cd and $\{Cd^{2+}\}$ was consistent and was successfully described for all data, irrespective of contact time, or desorption history, by a single Freundlich isotherm ($k_F = 1.38 \pm (0.024) \times 10^3$; $n = 0.672 \pm 0.01$). The model lines in Figs. 2 and 3 represent the optimised kinetic model (Eqs. (6) and (8); $R^2 = 0.999$) fitted simultaneously to all the sorption and desorption data. The model parameters k_F, k_1, and k_{-1} were parameterised using all sorption, desorption and solution data (Cd_{LS} and $\{Cd^{2+}\}$) shown in Figs. 2 and 3 as a single dataset. The rate constant of the forward reaction ($k_1 = 0.045 \pm 0.002\ d^{-1}$) was only slightly smaller than that for the backwards reaction ($k_{-1} = 0.062 \pm 0.003\ d^{-1}$) and the half-life ($t_{1/2}$) of the reversible reaction was only 6.5 d. These results suggest a comparatively short residence time of Cd in the *CaY* lattice and that the majority of initially sorbed Cd^{2+} remained isotopically exchangeable. For example ~63% of total sorbed Cd remained labile at $t > 40$ d (Fig. 4). If *CaY* represented a 'zero-sink' (i.e., the reaction proceeded only with the forward reaction with $k_1 = 0.045\ d^{-1}$) then $t_{1/2}$ for the reaction would be ~15 d. The kinetic model assumed a two-step Cd fixation process where Cd^{2+} ions transfer to a non-labile form following initial sorption to labile sites. Direct transfer of Cd^{2+} from the solution phase to non-labile sites is another possible fixation pathway. Unfortunately, we are not able to dif-

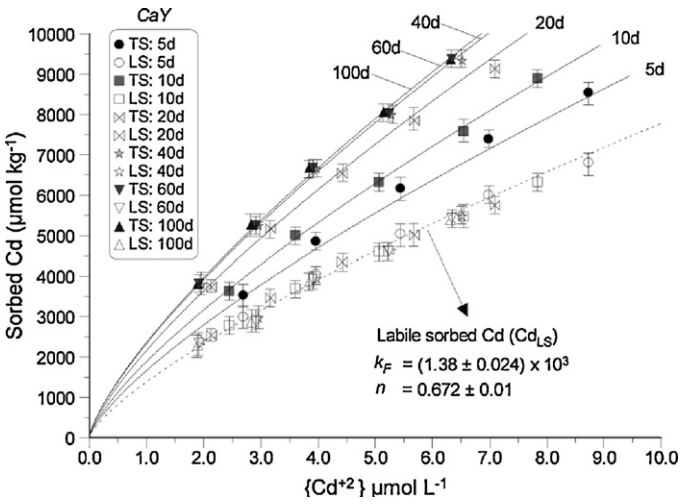

Fig. 2. Time-dependent Cd sorption, as a function of $\{Cd^{2+}\}$, by *CaY*. Solid lines represent the kinetic-adsorption model fitted to the total sorbed (TS) Cd data; the dotted line represents the same model fitted to the labile sorbed (LS) Cd data.

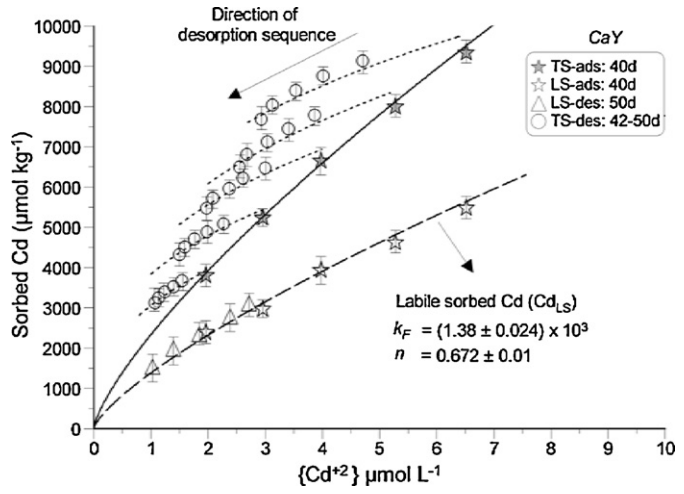

Fig. 3. Cadmium sorption and desorption on *CaY*, as a function of $\{Cd^{2+}\}$, following 40 d equilibration. Closed star symbols (★) represent total sorbed (TS-ads) Cd following adsorption; open circles (◯) represent subsequent desorption. Labile sorbed (LS-ads) Cd is shown following adsorption (☆) and desorption (△). The solid and dashed lines represent the kinetic-adsorption model fitted to total and labile sorption data at 40 d; the dotted lines represent the same model fitted to desorption data. The model was parameterised once only, using all the data shown in this figure.

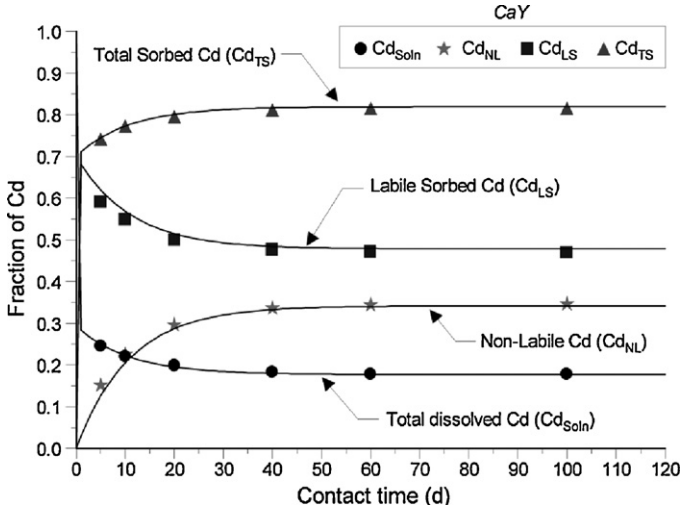

Fig. 4. Fitted curves (solid lines) obtained from modelling simulations (up to 100 d) for the sorption and fixation kinetics of Cd on *CaY*. Symbols represent experimental data for Cd_{soln}, Cd_{TS}, Cd_{LS}, and Cd_{NL}.

ferentiate between the two mechanisms using the current data alone and hence a definite identification of Cd fixation route is not possible. In this study the maximum concentration of added Cd (up to 12 mmol Cd kg^{-1}) was only 0.56% of the CEC of *CaY* (~4258 mmol kg^{-1}).

As shown in Fig. 4, after a contact time ≥40 d, with an apparent equilibrium between labile and non-labile forms of Cd, ~30–35% of initially loaded Cd was fixed whereas ~63% remained labile. The amount of Cd fixed by *CaY* was much less than that fixed by *CaX* ($Cd_{NL} \approx 80\%$; SAR = 1.3) in our previous study carried out using a similar experimental approach and conditions [25]. In addition, Cd_{NL} reached an asymptote after about 45 d, which is much faster than for *CaX*. Thus, although Cd sorption by *CaY* is clearly affected by ageing time, the kinetic barrier to reversible desorption was considerably less than in the case of *CaX*, as shown visually by the greater desorbability (Fig. 3) and numerically by the short half-life for transfer between 'fixed' and 'labile' forms.

As shown in Fig. 5a and b, the CM model (i.e., Eq. (13)) was found to give a good fit ($R^2 = 0.99$) to measured Cd_{NL} data with $D = 4.2 \times 10^{-13}$ m^2 s^{-1}, $D_1 = 2.5 \times 10^{-12}$ m^2 s^{-1}, $\zeta = 1.6 \times 10^{-6}$ s^{-1} and $\alpha = 0.219$. The parameter ζ represents the first-order rate constant for Cd^{2+} ions migration from the small cages into the large cavities; this value is close to that of the backward rate constant of the KM model ($k_{-1} = 7.18 \times 10^{-7}$ s^{-1}). At $t \to \infty$, the slope of the linear asymptote ($B_m t$ *vs* $U(t)$) $\approx \zeta \cong 1 \times 10^{-6}$. This indicates that Cd sorption kinetics within the *CaY* occurs in two kinetically distinct steps and that the mechanism is a coupled (rapid) diffusion and intracrystalline cation exchange process. The values of the parameters α, ζ and D are in reasonable agreements with those obtained in the study of Brown and Sherry [39,40].

3.3. Kinetics of cadmium sorption on clinoptilolite (*CaCpt*)

Temporal changes in Cd sorption by *CaCpt* up to 50 d are shown in Fig. 6; results show comparatively limited time-dependent sorption. Beyond a contact time of 25 d, further Cd sorption is very slow and the amount of fixed Cd is virtually constant at ~30% (Fig. 7). This suggests limited access to internal sites (non-labile sites) in the *CaCpt* matrix. The relationship between $\{Cd^{2+}\}$ and Cd_{LS} for all sorption data was described by a single adsorption isotherm. As shown in Table 3, the Langmuir isotherm ($R^2 = 0.999$) described this relationship better than Freundlich isotherm ($R^2 = 0.997$). However, the optimised value of q_{max} (2.74 mmol kg^{-1}) obtained was far less than the calculated CEC value for *CaCpt* (2670 mmol kg^{-1})

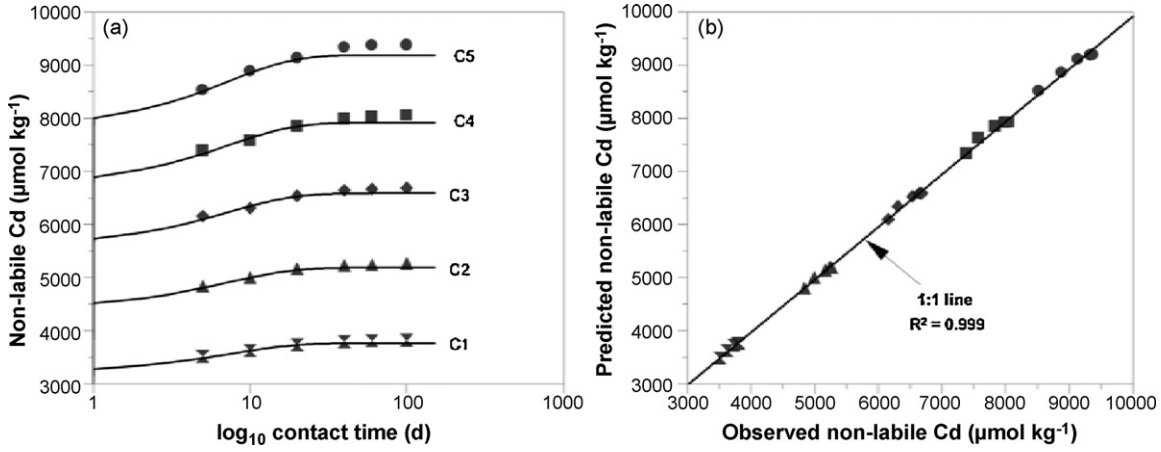

Fig. 5. Coupled ion exchange-diffusion (CM) model (a) CM model (solid line, Eq. (13)) fitted to experimental data (symbols) of Cd_{NL} for the Cd-CaY system and (b) 1:1 line for measured (Cd_{NL}) data *vs* model predictions.

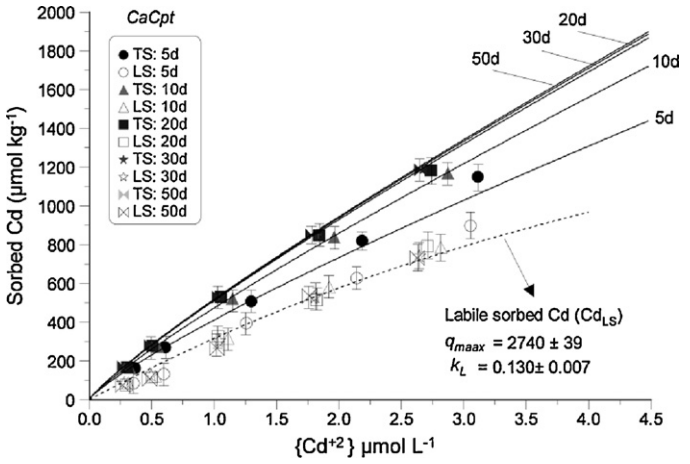

Fig. 6. Time-dependent Cd sorption, as a function of $\{Cd^{2+}\}$, by *CaCpt*. Solid lines represent the kinetic model, based on a Langmuir isotherm, fitted to the total sorbed Cd data; the single dotted line represents the same model fitted to the labile sorbed Cd data.

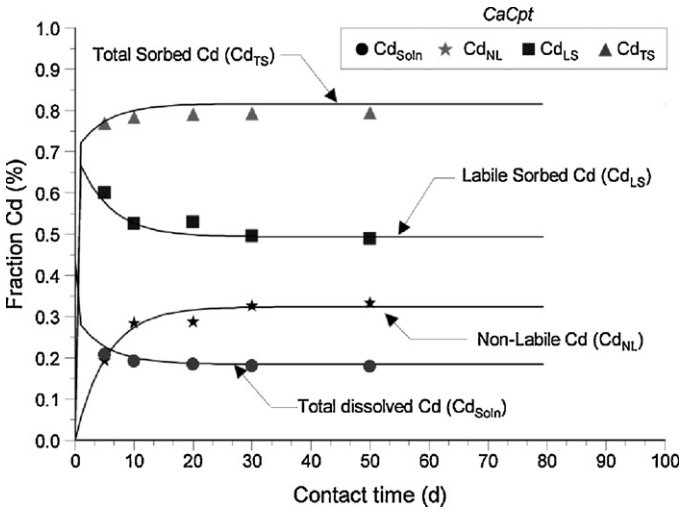

Fig. 7. Fitted curves (solid lines) obtained from modelling simulations (up to 50 d) for the sorption and fixation kinetics of Cd on *CaCpt*. Symbols represent the experimental data of Cd_{soln}, Cd_{TS}, Cd_{LS}, and Cd_{NL}.

Table 3
Values of optimised parameters of the kinetic model fitted to experimental data of *CaCpt*.

	Kinetic model Langmuir	Kinetic model Freundlich
R^2	0.999	0.997
k_1	0.086 ± 0.002	0.194 ± 0.017
k_{-1}	0.131 ± 0.004	0.172 ± 0.018
	q_{max} = 2740 ± 39	k_{FL} = 251 ± 7
Other parameters	k_L = 0.130 ± 0.007	n = 0.999 ± 0.030

which may be a fitting artefact arising from the small Cd loading used compared to the maximum sorption capacity of *CaCpt* or may indicate the presence of a specific sub-group of sites. In contrast to the *CaY* data, the Freundlich exponent (n) was virtually 1.0 (Table 3) which suggests minimal site heterogeneity. The solid lines in Fig. 6 represent the best fit (k_L, q_{max}, k_1, and k_2; R^2 = 0.999) of the KM model (Eqs. (7) and (8)) fitted to the sorption data only. The half-life of the reversible reaction was only 3.2 d which suggests a short residence time of Cd in the clinoptilolite lattice and that the majority of initially sorbed Cd^{2+} remained isotopically exchangeable. Unfortunately, it was not possible to apply the same kinetic model to desorption data due to a relatively high error in the determination of Cd_{soln} (data not shown). Obtaining reproducible batch samples from the natural zeolite samples was difficult, possibly due to phase heterogeneity (~80% clinoptilolite existed together with other phases such as quartz, smectite, illite and feldspar) and the wide range of particle size distribution. If *CaCpt* represents a Cd 'zero-sink' with $k_1 = 0.086\ d^{-1}$ then $t_{1/2}$ for the reaction would be ~8.1 d.

As shown in Fig. 8a and b, the CM model (i.e., Eq. (13)) was found to give a reasonably good fit (R^2 = 0.89) to measured Cd_{NL} data. The model predicted an apparent Cd diffusivity $D = 5.7 \times 10^{-12}\ m^2\ s^{-1}$ and $D_1 = 5.2 \times 10^{-11}\ m^2\ s^{-1}$. The value of ζ ($1.5 \times 10^{-6}\ s^{-1}$) was very small indicating that the limiting step for Cd sorption is the intracrystalline ion exchange and not diffusion. This conclusion is further supported by the fact that as $t \to \infty$, the slope of the linear asymptote ($B_m t$ *vs* $U(t)$) approaches a value of 2.5×10^{-5}. The predicted values of ζ and the backward rate constant in the KM model ($k_{-1} = 1.99 \times 10^{-6}\ s^{-1}$) are fairly close ($\zeta/k_{-1} = 0.75$) which suggests a reasonable agreement between the CM and KM models. The predicted value of Cd diffusivity is smaller than that for Cu^{2+} given in previous studies [39] due to the smaller energy of hydration of the Cd^{2+} ions.

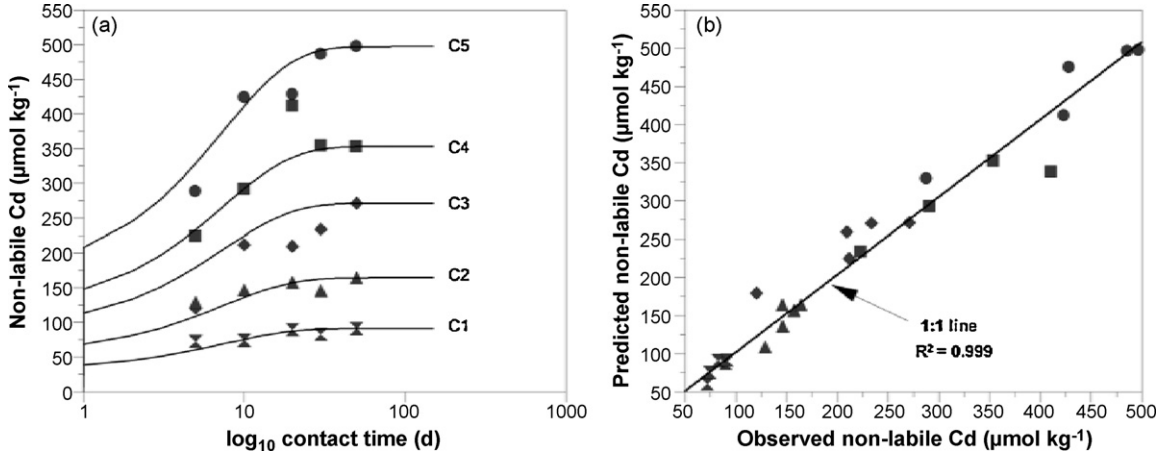

Fig. 8. Coupled ion exchange-diffusion (CM) model (a) CM model (solid line, Eq. (13)) fitted to experimental data (symbols) of Cd_{NL} for the Cd-*CaCpt* system and (b) 1:1 line for measured (Cd_{NL}) data *vs* model predictions.

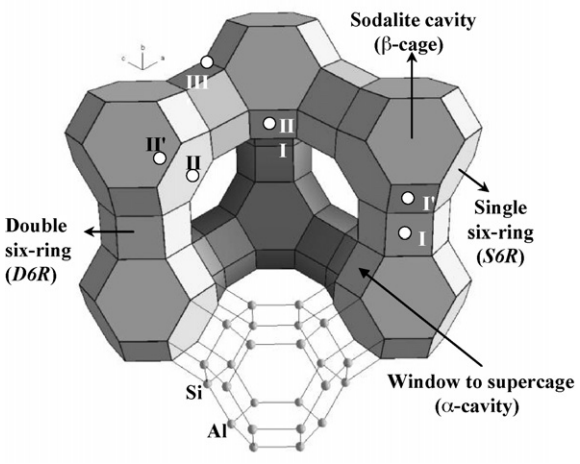

Fig. 9. A model of the Faujasite (X- or Y-zeolite) unit cell showing the distribution of extra-framework cations at exchange sites I, I′, II, II′, III, and III′, redrawn from Ref. [49].

3.4. Effect of zeolite crystal structure and the Si/Al ratio on Cd sorption

3.4.1. Y-type zeolite

The X- and Y-type zeolites are isostructural with faujasite (a naturally occurring zeolite) but differ in composition (Fig. 9) [5]. While X-zeolite have an Si/Al ratio of <1.5, Y-zeolite spans a Si/Al ratio of 1.5–3.8 [40,41]; increasing substitution of Al^{3+} leads to increased charge density in the zeolites pores. The high SAR (2.6) of the *CaY* material (low charge density) would create a higher energy barrier for the transport of Cd^{2+} ions from solution into non-labile sites (i.e., site I in Fig. 9). This may explain the time-dependant Cd^{2+} sorption reported in this study. In-line with findings from our recent study [31], non-labile Cd is expected to reside in site I of the Y-zeolite crystal. This means that the majority of labile Cd is expected to reside in the large cavities (i.e., sodalite and α-cavity in Fig. 9) and to a lesser extent at the external surface of the zeolite framework; this pool of labile Cd is in direct contact with the solution phase and can be desorbed easily.

3.4.2. Clinoptilolite

Clinoptilolite is a high-silica (Si/Al ≥ 4.0) variety of heulandite (HEU). The clinoptilolite framework is composed of dense layers parallel to the (0 1 0) *hkl* plane and its structure consists fundamentally of a building unit called 1,3 stellated cube (Fig. 10a) [42,43]. Clinoptilolite has a two-dimensional channel system consisting of three types of channels. Two channels are parallel to the *hkl* (0 0 1) plane and comprise 10-membered C_I rings (channel C_I) and 8-membered C_{II} rings (channel C_{II}). The third channel (C_{III}) is parallel to the *hkl* (1 0 0) plane and consists of 8-membered C_{III} rings (Fig. 10a and b). There are four cation exchange sites; S_I, S_{II}, S_{III} and S_{IV} located in channels C_I, C_{II}, C_{III}, and the centre of the inversion of channel C_I, respectively (Fig. 10a) [44]. The free aperture of the rings C_I, C_{II} and C_{III} in hydrated heulandite-type zeolites are 4.4×7.2, 4.1×4.7 and 4.0×5.5 Å, respectively [45]. This bi-dimensional channel system of clinoptilolite creates two types of cages; the first is formed from two C_{II} rings and two C_{III} rings while the second cage is formed from two C_I rings and two C_{III} rings. With all channels running parallel to the (0 1 0) direction, it is reasonable to assume that cation diffusion occurs only in this direction. Cation diffusion perpendicular to the (0 1 0) direction requires the penetration of tetrahedral five-membered rings which maybe unfavourable. Yang and Armbruster [46] refined the structure of Cs-exchanged heulandite and revealed the penetration of Cs^+ in the channel system of heulandite and the decrease of zeolitic H_2O molecules with increasing Cs^+ exchange due to limited space in structural pores. They also reported an increase in unit cell dimensions for the $Cs^+ \rightarrow Na^+$ exchange at 100 K which indicates the flexibility of the heulandite framework structure. Cs^+ has a large radius of hydration (Cs^+–H_2O bond length = 2.95 Å), and yet it diffuses into the pores of heulandite crystals. Hydrated Cd^{2+} ions have a regular octahedral structure with a Cd^{2+}–H_2O bond length of 2.29 Å (i.e., radius = 4.58 Å) which is much smaller than that of Cs^+ which suggests that Cd^{2+} can diffuse into the internal pore structure of clinoptilolite. Since the C_{III} ring has the smallest free diameter of the clinoptilolite structure, hydrated Cd^{2+} may prefer to diffuse *via* C_I or C_{II} leading to an anisotropic diffusion (i.e., directionally dependent). The energy of hydration (ΔH_{hyd}) of the ions Pb^{2+}, Cd^{2+}, Mn^{2+}, Zn^{2+}, Cu^{2+} and Ni^{2+} follows the order $-1495 < -1799 < -2002 < -2025 < -2084 < -2159$ kJ mol^{-1}. The selectivity of these ions for exchange by clinoptilolite follows the order of decreasing ΔH_{hyd}. This means that the relatively weak electrostatic field within clinoptilolite is able to strip water of hydration from Pb^{2+} and Cd^{2+} to overcome any steric hindrance at the 8-membered rings; this is less likely in the case of elements such as Cu^{2+} and Ni^{2+}. Partial dehydration can explain the irreversible sorption of Cd within selected site locations. Another possible explanation for Cd fixation is that hydrated Cd^{2+} ions can freely exchange at site S_{IV} in the fourth channel. Since site S_{IV} is located in a small side of the inversion channel then we would

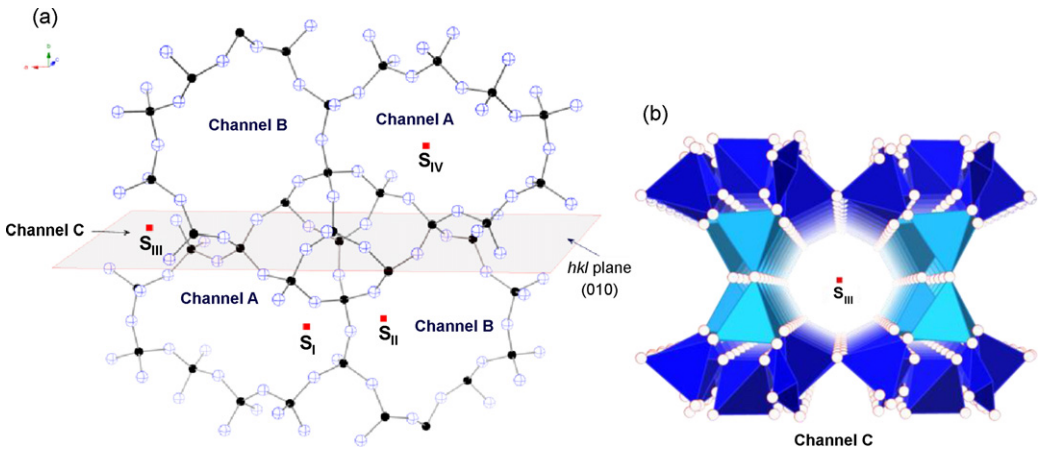

Fig. 10. Structure of clinoptilolite unit cell: (a) projection along the (0 0 1) *hkl* plane illustrating channel C_I (10-membered ring) and channel C_{II} (8-membered ring) and the positions of the preferential exchange sites (S_I, S_{II}, S_{III} and S_{IV}) occupied by cations (after Ref. [43]) and (b) projection along (1 0 0) *hkl* plane illustrating channel C_{III} comprised of 8-membered rings (see Ref. [44]).

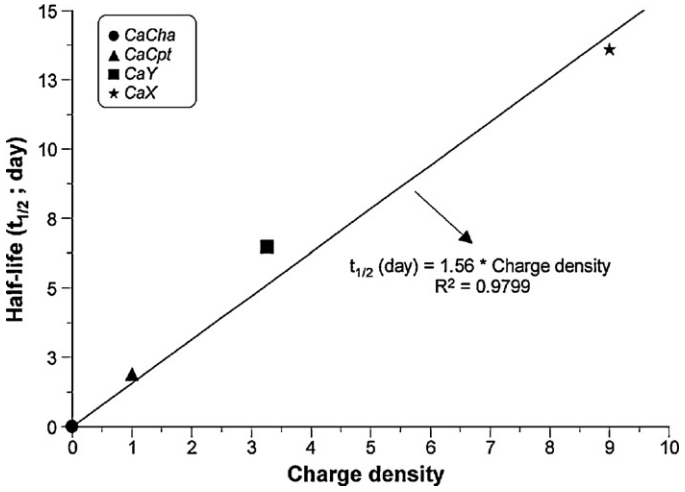

Fig. 11. Charge density of non-labile sites (per unit cell) *vs* half-life of the non-labile desorption reaction ($t_{1/2}$; Eq. (9)) for *CaX* (⋆), *CaY* (■), *CaCpt* (▲), and *CaCha* (●). Charge density and $t_{1/2}$ of *CaCha* are assumed zero.

expect minor occupancy of Cd^{2+} at this site and thus a small proportion of Cd^{2+} ions that are only slowly exchangeable ('fixed'). Site S_{IV} is a highly specific location and removing Cd^{2+} from this site into solution is expected to be associated with large entropy changes. Although the open framework system of clinoptilolite suggests a reversible sorption mechanism, previous studies that support our findings reported incomplete ion exchange and cation release, even after washing or treatment with NaCl or HCl, suggesting the incorporation of cations within the solid matrix [47–49,8].

Olson [50] reported an occupancy of 9 Na^+ ions in site I (per unit cell) for hydrated X-zeolite (SAR = 1.18) at 25 °C, whereas Marti et al. [51] reported an occupancy of only 3.27 Na^+ ions in site I (per unit cell) of hydrated Y-zeolite (SAR = 2.36) at 25 °C. If we accepted that local inhomogeneity in SAR distribution which comes from cation distribution is negligible then Cd fixation is directly linked to Cd^{2+} occupancy in site I for both *CaX* and *CaY* and one possible non-labile site is available in the *CaCpt* unit cell. Ahmed et al. [25] showed that Cd sorption by chabazite (*CaCha*; SAR = 3.1) is completely reversible and assumed the absence of any non-labile sites in this material. Fig. 11 shows a linear correlation between charge density of the non-labile sites – given above – for *CaX*, *CaY*, *CaCpt*, and *CaCha vs* the half-life of the non-labile desorption reaction ($t_{1/2}$; Eq. (9)). A cation in site I in Faujasite-type zeolites is surrounded by almost twice the number of T-atoms that surround any cation in site I′ or II. Thus it is reasonable to expect that the change in SAR would not affect different types of sites equally. However, the data presented in Fig. 11 suggest that non-labile site exchange energy varies linearly with the average site density per unit cell especially for X- and Y-zeolites. This is in-line with the study of Van Dun et al. [52] which suggested that differences in site energy levels vary linearly with the average number of Al atoms per units cell. These authors showed reversal site preference in Faujasite-type zeolites from I > II > I′ to II > I′ > I that takes place with increasing SAR. This result agrees well with our proposal for the "electrostatic trap" in small pores [31] as an explanation for metal fixation in low silica zeolites and the limited Cd fixation in highly siliceous zeolites as demonstrated in this study.

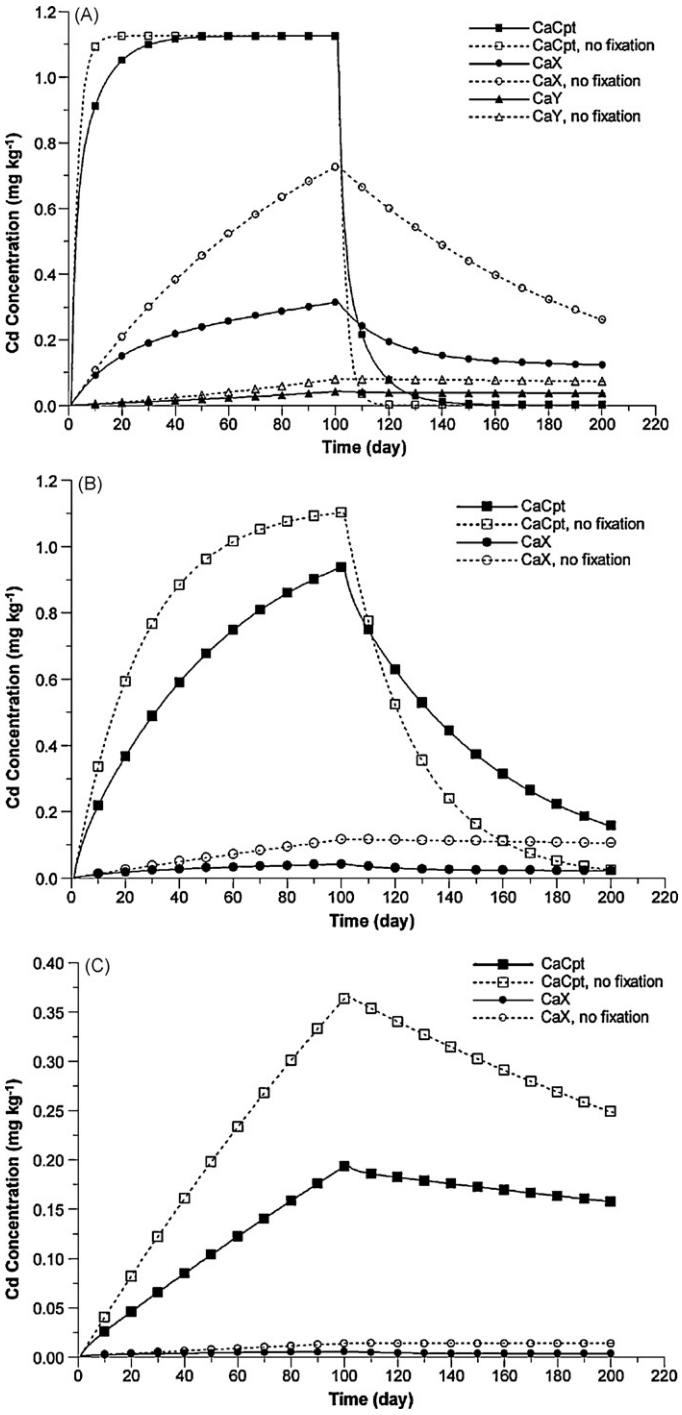

Fig. 12. Simulation of Cd attenuation by PRBs containing a 10 cm layer of clinoptilolite (■), X-Zeolite (●) or Y-zeolite (▲). Lateral water fluxes are (a) 10^4 (b) 10^3 and (c) 10^2 L m^{-2} d^{-1}. The trends show the effect of a 100-d input pulse of 10^{-5} M Cd against a long-term steady state concentration of 10^{-8} M Cd in the PRB eluent. Freundlich parameters and rate constants governing fixation for each zeolite are given in Table 4. Solid lines show the effect of equilibrium between labile adsorbed and solution Cd only; broken lines include the additional effect of time-dependent Cd fixation. *Note*: Y-zeolite is omitted from (b) and (c) as the data series are indistinguishable from the horizontal axis.

3.5. Outlook: the role of reversible metal fixation in Permeable Reactive Barriers

Permeable Reactive Barriers (PRBs) containing metal-sorbing materials can protect water systems against lateral flow of metal-contaminated leachate [53,54]. However, under conditions of continuous flow at elevated metal concentration the PRB's capacity to attenuate contaminants would decline as the adsorbent reached equilibrium with the incoming metal concentration. A secondary, but related, function of the PRB is to moderate potentially harmful transient pulses in effluent metal concentration where contamination is intermittent. In this context, the ability of zeolites to

Table 4
Values of optimised parameters of the kinetic model based on Freundlich isotherm fitted to experimental data of *CaX*, *CaY* and *CaCpt*.

Material	$k_1 \times 10^{-3}$ (d^{-1})	$k_{-1} \times 10^{-3}$ (d^{-1})	$k_F \times 10^3$ ($L\,kg^{-1}$)	n
CaX	42.0 ± 0.61	9.00 ± 0.22	12.1 ± 0.290	1.02 ± 0.013
CaY	45.0 ± 2.00	62.0 ± 3.00	1.38 ± 0.024	0.672 ± 0.01
CaCpt	194 ± 17.0	172 ± 18.0	0.251 ± 0.007	0.999 ± 0.030

'reversibly fix' metals may provide the additional benefit of delaying the release of adsorbed metal, following the passage of a high metal concentration pulse. Fig. 12a–c shows the simulated trend in Cd concentration in water passing through a PRB containing a 10 cm thick layer (density 1000 $kg\,m^{-3}$) of the zeolites *CaCpt*, *CaX* or *CaY* at water fluxes of 10^2, 10^3 or 10^4 $L\,m^{-2}\,d^{-1}$. The Freundlich constants for labile Cd adsorption and the rate constants governing fixation and release of non-labile Cd (Table 4) were applied in the model using a dynamic time step of 1 d. The simulation imposed a transient spike of 10^{-5} M Cd for 100 d against a background concentration in the groundwater of 10^{-8} M.

The trends shown strongly reflect the different buffer capacities of the zeolites. In Fig. 12a the high water flux of 10^4 $L\,m^{-2}\,d^{-1}$ quickly exhausted the buffer capacity of *CaCpt*: the Cd concentration in the effluent equalled that of the pulse within 10 d and the additional effect of temporary fixation was negligible. By contrast, for *CaX* the duration of the pulse was insufficient to establish a steady state and the additional moderating influence of fixation was clear in reducing the peak Cd concentration by more than 50%. In Fig. 12b the slower water flux revealed an important feature of the moderating influence of temporary Cd fixation: when the fixation of *CaCpt* acts to *delay* the outflow of Cd, not to eliminate it through permanent sorption. Thus, after the passage of the Cd pulse the concentration of Cd in the PRB effluent actually exceeded that of the clinoptilolite with no assumed fixation capability. Therefore, the benefit from temporary fixation lies in the overall moderation of the Cd concentration so that aquatic life would be subjected to a more prolonged period of low Cd concentration rather than a shorter period of exposure to high concentration. Fig. 12c shows the performance of *CaCpt* with a relatively minor challenge from a spike flux 100 $L\,m^{-2}\,d^{-1}$, equivalent to a layer of water equal to the thickness of the PRB-zeolite layer. In this case, the peak concentration reached was reduced by 50% due to reversible fixation and to 1/6th of the Cd concentration in the incoming pulse. Both *CaX* and *CaY* zeolites effectively eliminated the Cd pulse. The reversibility of Cd fixation means that, in all cases, the Cd would continue to leak from the PRB at low concentration into the surrounding environment, which is clearly undesirable. However, this gradually returns the functionality of the PRB to moderate future pulses of high metal concentration.

4. Conclusions

This study showed that equilibrating Cd with *CaY* and *CaCpt* for up to 40 d caused a progressive increase in the concentration of sorbed Cd but no change in the equilibrium of isotopically exchangeable Cd, as found previously for X-zeolite. Slow sorption kinetics beyond 5 d is believed to be due to electrostatic trapping of Cd in small pores in *CaY* and *CaCpt* lattices. However, desorption experiments, and results from a fitted kinetic model, suggest a relatively short residence time for Cd in a 'fixed' state. Results from the two-state kinetic model and the coupled ion exchange-diffusion model were in reasonable agreement for both *CaY* and *CaCpt* which indicate that the cation fixation and release from small ports in zeolites are kinetically controlled processes especially when metal ions are present in trace amounts.

Most zeolites are relatively insoluble over a wide pH range (3–10); their dissolution by specialised bacteria occurs at an extremely slow rate [55]. These characteristics and their comparative ease of handling make zeolites suitable candidates as reactive media for PRBs. However, the potential desorption or reverse ion exchange of metals must be considered if zeolites are used as barriers in protecting groundwaters from inorganic contamination. Our kinetic model, describing sorption and reversible fixation, suggests that continued flushing of zeolites within a PRB, following transition of a high metal concentration pulse, leads to gradual discharge of initially fixed metal. The primary role of the zeolite in this context is therefore to protect aquatic ecosystems from elevated pulses of trace metals by delaying the release of these contaminants—rather than permanent and irreversible removal. Considering such a regenerative capacity for metal sorption, their stability and low cost, zeolites may have a useful role in PRB when coupled with other sorbents such as zero-valent iron.

Acknowledgments

Authors are thankful to the University of Nottingham for providing support for this research. Thanks are also extended to the technical support at the Environmental Science division, School of Biosciences, Nottingham University.

Appendix A. Supplementary data

Supplementary data associated with this article can be found, in the online version, at doi:10.1016/j.jhazmat.2010.08.074.

References

[1] M.N.V. Prasad, K.S. Sajwan, R. Naidu, Trace Elements in the Environment: Biogeochemistry, Biotechnology, and Bioremediation, CRC, 2005.
[2] E.J. Calabrese, A.T. Canada, C. Sacco, Annual Review of Public Health 6 (1985) 131.
[3] B. Sarkar, Heavy Metals in the Environment, Marcel Dekker, Inc., New York, 2002.
[4] J.V. Smith, Microporous and Other Framework Materials with Zeolite-type Structures: Tetrahedral Frameworks of Zeolites, Clathrates and Related Materials, Springer-Verlag, Berlin, 2000.
[5] T. Frising, P. Leflaive, Microporous Mesoporous Materials 114 (2008) 27.
[6] S.M. Auerbach, K.A. Carrado, P.K. Dutta, Handbook of Zeolite Science and Technology, Marcel Dekker, New York, 2003.
[7] A.E. Osmanlioglu, Journal of Hazardous Materials 137 (2006) 332.
[8] K. Gedik, I. Imamoglu, Journal of Hazardous Materials 155 (2008) 385.
[9] U. Wingenfelder, C. Hansen, G. Furrer, R. Schulin, Environmental Science & Technology 39 (2005) 4606.
[10] W. Qiu, Y. Zheng, Chemical Engineering Journal 145 (2009) 483.
[11] H.S. Sherry, S.M. Auerbach, K.A. Carrado, P.K. Dutta, Handbook of Zeolite Science and Technology, Marcel Dekker, Inc., New York, 2003, p. 1007.
[12] C. Colella, Mineralium Deposita 31 (1996) 554.
[13] F. Helfferich, Ion Exchange, McGraw-Hill, Inc., New York, 1962.
[14] D. Ming, E. Allen, Reviews in Mineralogy and Geochemistry 45 (2001) 619.
[15] D. Ruthven, in: H.G. Karge, J. Weitkamp (Eds.), Adsorption and Diffusion, Springer-Verlag, Berlin, 2008, p. 1.
[16] P. Fletcher, R.P. Townsend, Journal of Chromatography 238 (1982) 59.
[17] P.P. Lai, L.V.C. Rees, Journal of the Chemical Society-Faraday Transactions I 72 (1976) 1809.
[18] B.H. Wiers, R.J. Grosse, W.A. Cilley, Environmental Science & Technology 16 (1982) 617.
[19] R.M. Barrer, J.A. Davies, L.V.C. Rees, Journal of Inorganic & Nuclear Chemistry 31 (1969) 219.
[20] R.M. Barrer, L.V.C. Rees, R.F. Bartholomew, Journal of Physics and Chemistry of Solids 24 (1963) 51.
[21] M. Trgo, J. Perić, Journal of Colloid and Interface Science 260 (2003) 166.
[22] P. Fletcher, R.P. Townsend, Journal of the Chemical Society-Faraday Transactions 1 81 (1985) 1731.
[23] J.G. Nery, Y.P. Mascarenhas, A.K. Cheetham, Microporous and Mesoporous Materials 57 (2003) 229.
[24] J.F. O'Connor, R.P. Townsend, Zeolites 5 (1985) 158.
[25] I.A.M. Ahmed, S.D. Young, N.M.J. Crout, Geochimica et Cosmochimica Acta 70 (2006) 4850.
[26] I.A.M. Ahmed, N.M.J. Crout, S.D. Young, Geochimica et Cosmochimica Acta 72 (2008) 1498.

[27] O.P. Mehra, M.L. Jackson, Clay and Clay Minerals 7 (1958) 317.
[28] M. Pansu, J. Gautheyrou, Handbook of Soil Analysis: Mineralogical, Organic and Inorganic Methods, Springer, Heidelberg, 2006.
[29] T.E. Cook, W.A. Cilley, A.C. Savitsky, B.H. Wiers, Environmental Science & Technology 16 (1982) 344.
[30] H. Robson, Verified Syntheses of Zeolitic Materials, Elsevier Science B.V., Amsterdam, The Netherlands, 2001.
[31] I.A.M. Ahmed, S.D. Young, J.F.W. Mosselmans, N.M.J. Crout, E.H. Bailey, Geochimica et Cosmochimica Acta 73 (2009) 1587.
[32] J.W. Ball, D.K. Nordstrom, User's Manual for WATEQ4F, With Revised Thermodynamic Database and Test Cases for Calculating Speciation of Major, Trace and Redox Elements in Natural Waters, U.S. Geological Survey Open-File Report 91-183, Denver, Colorado, 1991.
[33] J.H. Strickland, T.R. Parsons, A Practical Handbook of Seawater Analysis, vol. Bulletin 167, Fisheries Research Board of Canada, 1968.
[34] L.S. Clescerl, A.E. Greenberg, A.D. Eaton, Standard Methods for Examination of Water & Wastewater, American Public Health Association, Washington, DC, 1999.
[35] W.H. Press, S.A. Teukolsky, W.T. Vetterling, B.P. Flannery, Numerical Recipes: The Art of Scientific Computing, Cambridge University Press, Cambridge, UK, 2007.
[36] M.D. Baker, C. Senaratne, J. Zhang, The Journal of Physical Chemistry 98 (1994) 1668.
[37] L.M. Brown, H.S. Sherry, F.J. Krambeck, Journal of Physical Chemistry 75 (1971) 3846.
[38] H. Faghihian, H. Kazemian, M. Maragheh, Journal of Radioanalytical and Nuclear Chemistry 242 (1999) 491.
[39] I. Rodríguez Iznaga, V. Petranovskii, G. Rodríguez Fuentes, C. Mendoza, A. Benítez Aguilar, Journal of Colloid and Interface Science 316 (2007) 877.
[40] D.W. Breck, Journal of Chemical Education 41 (1964) 678.
[41] P.A. Jacobs, E.M. Flanigen, J.C. Jansen, H. van Bekkum, Introduction to Zeolite Science and Practice, Elsevier, Amsterdam, The Netherlands, 2001.
[42] A. Godelitsas, T. Armbruster, Microporous and Mesoporous Materials 61 (2003) 3.
[43] S.X. Han, J.V. Smith, Acta Crystallographica Section A 50 (1994) 302.
[44] K. Koyama, Y. Takeuchi, Zeitschrift fur Kristallographie 145 (1977) 216.
[45] W.J. Mortier, J.R. Pearce, American Mineralogist 66 (1981) 309.
[46] P. Yang, T. Armbruster, Journal of Solid State Chemistry 123 (1996) 140.
[47] M. Culfaz, M. Yagiz, Separation and Purification Technology 37 (2004) 93.
[48] V.J. Inglezakis, M.D. Loizidou, H.P. Grigoropoulou, Water Research 36 (2002) 2784.
[49] A. Langella, M. Pansini, P. Cappelletti, B. de Gennaro, M. de'Gennaro, C. Colella, Microporous and Mesoporous Materials 37 (2000) 337.
[50] D.H. Olson, Journal of Physical Chemistry 74 (1970) 2758.
[51] J. Marti, J. Soria, F.H. Cano, Journal of Colloid and Interface Science 60 (1977) 82.
[52] J.J. Van Dun, K. Dhaeze, W.J. Mortier, D.E.W. Vaughan, Journal of Physics and Chemistry of Solids 50 (1989) 469.
[53] D.W. Blowes, C.J. Ptacek, S.G. Benner, C.W.T. McRae, T.A. Bennett, R.W. Puls, Journal of Contaminant Hydrology 45 (2000) 123.
[54] D. Naftz, S.J. Morrison, C.C. Fuller, J.A. Davis, Handbook of Groundwater Remediation using Permeable Reactive Barriers: Applications to Radionuclides, Trace Metals and Nutrients, Academic Press, 2002.
[55] C. Zhu, Geochimica et Cosmochimica Acta 69 (2005) 1435.